Nano-Micro Lett. (2018) 10:27
https://doi.org/10.1007/s40820-017-0182-0

REVIEW

A Mini Review: Can Graphene Be a Novel Material for Perovskite Solar Cell Applications?

Eng Liang Lim[1] · Chi Chin Yap[1] · Mohammad Hafizuddin Hj Jumali[1] · Mohd Asri Mat Teridi[2] · Chin Hoong Teh[3]

Received: 23 October 2017 / Accepted: 5 December 2017 / Published online: 22 December 2017

Highlights

- Introduction of graphene improves photovoltaic properties of perovskite solar cells (PSCs).
- Graphene can be used as a conductive electrode, carrier transporting material, or stabilizer material.
- Graphene enhances the electrical properties and stability of PSCs.

Abstract Perovskite solar cells (PSCs) have raised research interest in scientific community because their power conversion efficiency is comparable to that of traditional commercial solar cells (i.e., amorphous Si, GaAs, and CdTe). Apart from that, PSCs are lightweight, are flexible, and have low production costs. Recently, graphene has been used as a novel material for PSC applications due to its excellent optical, electrical, and mechanical properties. The hydrophobic nature of graphene surface can provide protection against air moisture from the surrounding medium, which can improve the lifetime of devices. Herein, we review recent developments in the use of graphene for PSC applications as a conductive electrode, carrier transporting material, and stabilizer material. By exploring the application of graphene in PSCs, a new class of strategies can be developed to improve the device performance and stability before it can be commercialized in the photovoltaic market in the near future.

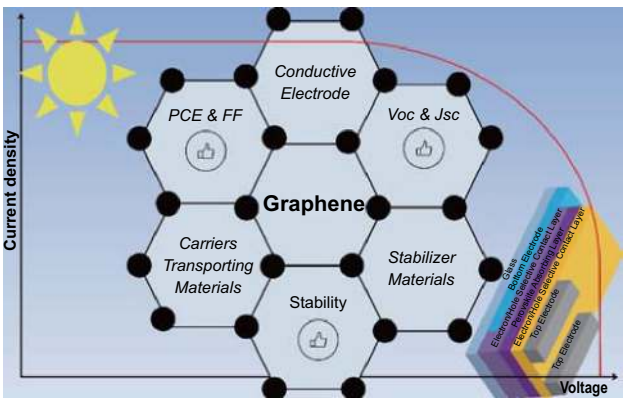

Keywords Perovskite solar cells · Graphene · Conductive electrode · Carrier transporting material · Stabilizer material · Performance and stability

✉ Eng Liang Lim
englianglim@ukm.edu.my

✉ Chi Chin Yap
ccyap@ukm.edu.my

[1] School of Applied Physics, Faculty of Science and Technology, Universiti Kebangsaan Malaysia, 43600 Bangi, Selangor, Malaysia

[2] Solar Energy Research Institute, Universiti Kebangsaan Malaysia, 43600 Bangi, Selangor, Malaysia

[3] ASASI Pintar Program, Pusat Permata Pintar Negara, Universiti Kebangsaan Malaysia, 43600 Bangi, Selangor, Malaysia

1 Introduction

Global climate change [1] and rapidly rising energy demand [2] require society to move toward sustainable and renewable energy resources. Among all sustainable and renewable energy resources, solar energy has potential to fulfill these needs because it is free and clean. Therefore, photovoltaic cells are extremely important for the conversion of solar energy into electricity. According to the latest survey, 90% of the photovoltaic products in the world market are based on first-generation crystalline (monocrystalline and polycrystalline) silicon (Si) wafers with power conversion efficiency (PCE) between 15 and 20% on the module level of 1.6 m^2 [3]. However, these cells are expensive due to the high cost of the processing and raw material of Si [4]. On the other hand, second-generation solar cells based on amorphous Si, cadmium telluride (CdTe), and copper indium gallium selenide (CIGS) did not repeat the success of the crystalline Si solar cells due to technological problems and the module stability issues [5, 6].

To overcome these problems, researchers need to explore new materials for next-generation photovoltaics. At present, perovskite solar cells (PSCs) have generated broad interest because of their rapid PCE improvement from 3.8% in 2009 to 22.1% in 2016 [7], as shown in Fig. 1a [8–14]. In addition, PSCs have the merits of low-cost processing, easy fabrication, and compatibility with flexible plastic substrates for large-area production [15, 16]. It should be noted that the certified efficiency of 16.0 ± 0.4% has been achieved for the minimodule PSC with the aperture area of 16.29 cm^2 [17]. Thus, PSCs have been considered as promising energy conversion candidates for carbon-free energy production in the next few years.

To date, several strategies such as electrode modification [18–21], metal-doping cathode buffer layer [22–25], surface modified perovskite layer [26–28], plasmonic nanoparticles [29–32], and introducing graphene-based materials within the device layers [33–37] have been carried out to boost the performance and stability of PSCs. In particular, integration of graphene into PSCs has attracted attention because graphene provides promising device designs with its potential low cost of production, high chemical stability, and appropriate energy level [38]. It should be noted that the efficiency of PSCs of over 18% has been achieved by using graphene-based materials (the highest reported efficiency of graphene PSCs to date) [39], indicating that graphene is a promising candidate for the development of PSCs. Graphene was discovered in 2004 by Russian-born scientists Andre Geim and Konstantin Novoselov utilizing, in the widely accepted terminology, the "Scotch tape method" [40].

It is well known that graphene is a name given to a two-dimensional (2D) sheet of sp^2 hybridized carbon atoms tightly packed into a 2D honeycomb crystal lattice. It can be stacked to form three-dimensional (3D) graphite, rolled to form one-dimensional (1D) nanotubes, and wrapped to form zero-dimensional (0D) fullerenes. Figure 1b illustrates graphene and its derivatives [41]. Its outstanding properties such as high thermal conductivity ($\sim 5 \times 10^3$ W m^{-1} K^{-1}) at room temperature [42], high charge carrier mobility (2×10^5 cm^2 V^{-1} S^{-1}) [43], high optical transparency (it absorbs 2.3% of the incident light in the range from infrared to violet) [44], large surface-to-mass ratio (2630 m^2 g^{-1}) [45], superior mechanical properties (i.e., Young's modulus of ~ 1 TPa) [46], and high flexibility have given it the potential to be used in various applications such as sensors [47], catalysts [48], optical modulators [49], surface-enhanced Raman spectroscopy (SERS) platforms [50], and optoelectronic devices (light-

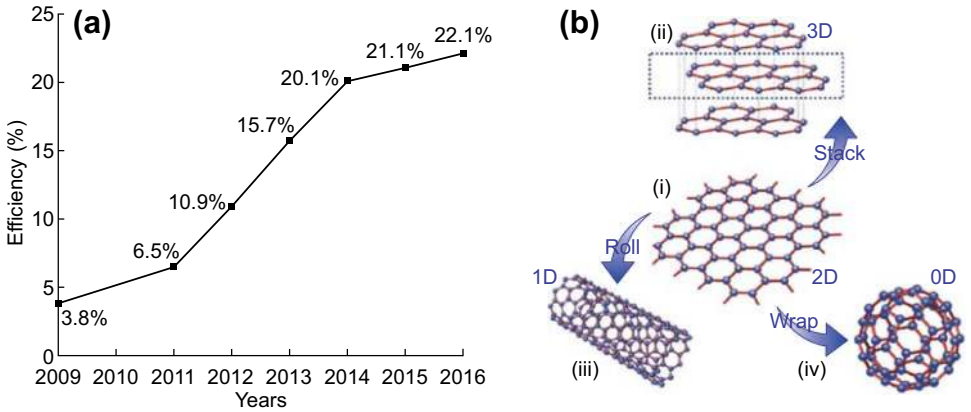

Fig. 1 **a** Evolution of PSC efficiencies from 2009 to 2016 [8–14]. **b** Graphene is a 2D hexagonal lattice of carbon atoms (i). It can be stacked into 3D graphite (ii), rolled into 1D nanotubes (iii), and wrapped into 0D buckyballs (iv). Reprinted with permission from Ref. [41] Copyright 2012 American Chemical Society

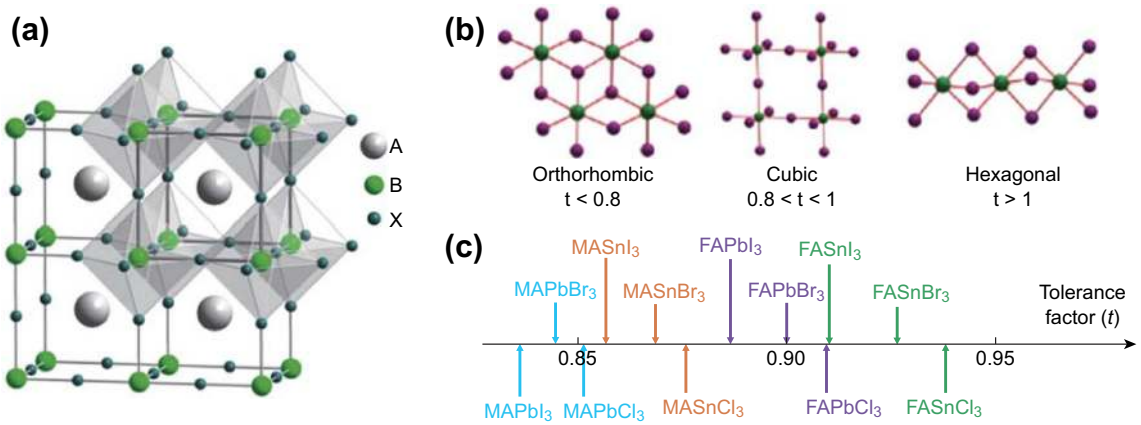

Fig. 2 **a** Basic ABX_3 perovskite crystal structure, reprinted with permission from [55] © 2008 American Physical Society. **b** Relationship between the tolerance factor, t, and the crystal structure of perovskite materials, reprinted with permission from [56] © 2016 American Chemical Society. **c** Tolerance factor of the different perovskite materials for perovskite solar cells applications, reprinted with permission from Ref. [58] Copyright 2015 The Royal Society of Chemistry

emitting diodes, solar cells, displays, touch screens) [51, 52].

Here, we present the successful application of graphene for high-performance and stable PSCs. Firstly, we introduce the crystal structure and tolerance factor of organic–inorganic perovskite materials. Secondly, we briefly introduce the working principle of PSCs. Thirdly, we highlight the progress of applying graphene for high-performance and stable PSCs. Finally, we provide the outlook and conclusion on the application of graphene for PSCs.

2 Crystal Structure and Tolerance Factor of Organic–Inorganic Perovskite Materials

The term "perovskite" is used when referring to a large compound group that has the same crystal structure as mineral perovskite $CaTiO_3$ [53]. For perovskite materials in solar energy applications, the basic building component is an ABX_3 crystal structure, where A represents an organic and/or inorganic cation such as methylammonium ($CH_3NH_3^+$ or MA^+), formamidinium ($NH(CH_3)_2^+$ or FA^+), or cesium (Cs^+), B represents a divalent metal cation (Pb^{2+} or Sn^{2+}), and X represents a halide anion (Cl^-, Br^-, or I^-) [13, 54]. The structures of the ABX_3 type are shown in Fig. 2a [55]. For a stable and formable ABX_3 perovskite structure, the tolerance factor, $t = (R_A + R_X)/\{\sqrt{2}(R_B + R_X)\}$ of perovskite materials should be close to 1 (corresponding to a perfectly packed perovskite structure), where R_A, R_B, and R_X are the effective ionic radii for A, B, and X ions, respectively.

It has been reported that organic–inorganic hybrid halide perovskite materials tend to form an orthorhombic structure if $t < 0.8$, cubic structure if $0.8 < t < 1.0$, and hexagonal structure if $t > 1$ [56], as shown in Fig. 2b.

Table 1 Estimation of A cation radii based on lead and/or tin trihalides perovskite materials, ABX_3

R_B (Å)	R_X (Å)	$R_A^{\#}$ (Å) at $t = 0.8$	$R_A^{\#}$ (Å) at $t = 1.0$
Pb^{2+} (1.19)	Cl^- (1.84)	1.59	2.44
	Br^- (1.96)	1.60	2.49
	I^- (2.20)	1.63	2.59
Sn^{2+} (1.18)	Cl^- (1.84)	1.58	2.43
	Br^- (1.96)	1.59	2.48
	I^- (2.20)	1.62	2.58

$^{\#}R_A$ (Å) $= t(\{\sqrt{2}(R_B + R_X)\}) - R_x$ (Å)

Based on the tolerance factor equation, the effective radii of Pb^{2+}, Sn^{2+}, Cl^-, Br^-, and I^- are 1.19, 1.18, 1.84, 1.96, and 2.20 Å [57], respectively. It is suggested that the organic or inorganic cation A with radius between 1.60 and 2.50 Å can form stable lead and/or tin halide perovskite structures at $0.8 < t < 1.0$ (see Table 1). Figure 2c shows the tolerance factor of the series of perovskite materials [58] that have been used for an absorbing layer in PSC applications. Other than the tolerance factor, the ionization energy of the organic–inorganic cation [59], dimensional phases of perovskite materials [60], chemical stability, valence band [58], etc., are also important for the formability and stability of perovskite structures.

3 Working Principle of PSCs

In general, the perovskite layer is composed of organic materials such as organic cations (i.e., methylammonium, ethylammonium, formamidinium) and inorganic materials such as metal cations (i.e., Pb^{2+}, Sn^{2+}, and Ge^{2+}) and halide anions (i.e., I^-, Cl^-, and Br^-). As a result, the working principle of PSCs has raised a number of questions

because the optical absorption of the perovskite layer cannot be distinguished. It should be noted that at the beginning of its discovery, PSCs were TiO_2-sensitized solar cells, using $MAPbI_3$ and $MAPbBr_3$ as sensitizers [8]. The free electrons excited after photon absorption by the sensitizer would be injected into the conduction band of the wide band gap TiO_2 inorganic semiconductor, followed by electron extraction to the transparent conductive oxide (TCO). The electrons would flow through the external circuit to the platinum (Pt) anode and then into the iodide electrolyte. The electrolyte would regenerate and transport the electrons back to the dye molecules. Therefore, it has been proposed that dye-sensitized solar cells (DSSCs) can be used as a model to explain the working mechanism of PSCs. Because of the dissolution issues of halides in a liquid electrolyte that could influence the stability of PSCs [9], the liquid electrolyte was replaced by a solid-state hole transporting material (i.e., Spiro-OMeTAD) [10].

In the case of PSCs, the perovskite material itself is an intrinsic (neither p-type nor n-type) semiconductor. Owing to the low binding energy of perovskite materials (2–55 meV [61, 62]), the free charge carriers (free electrons and free holes) formed inside the perovskite layer after photon absorption [61] can be quickly injected into electron/hole transporting materials with very slow charge carrier recombination and result in large values of the diffusion length [63]. Finally, the electrons/holes are extracted to the cathode/anode. Figure 3 illustrates the basic working mechanism of PSCs.

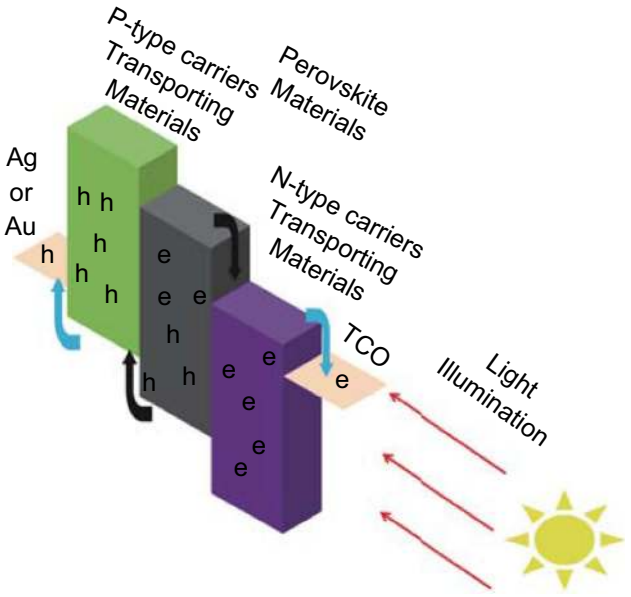

Fig. 3 General working mechanism of PSCs. Free charge carriers formed in the perovskite layer drift to the carrier transporting material (black arrow line), followed by charge extraction to the electrode (blue arrow line). (Color figure online)

4 Discussion

4.1 Graphene as Conductive Electrode

Recently, graphene has been successfully used as a conductive electrode for PSC applications [35, 64–67]. This was first reported by Yan et al. [65] using the lamination method for the chemical vapor deposition (CVD) produced graphene. Due to the high sheet resistance ($\sim 1050 \pm 150\ \Omega\ sq^{-1}$) of single-layer CVD-produced graphene films, a thin layer (~ 20 nm) of poly-(3,4-ethylenedioxythiophene):poly(styrenesulfonate) (PEDOT:PSSS) solution doped with fluorosurfactant Zonyl-FS300 together with D-sorbitol was spin-coated on top of the graphene surface to (1) reduce the graphene sheet resistance (2) act as an adhesion layer during the lamination process, and (3) induce more hole doping to the graphene electrode, since the Fermi level of PEDOT:PSS is higher than the graphene Dirac point. After optimizing the processing condition, the device performance with double-layer graphene films could achieve up to 12.37% efficiency, which is relatively high compared to that of the reported semitransparent TCO-free PSCs [68, 69]. The superior performance and high J_{sc} of the champion device originated from the low sheet resistance (Fig. 4a) and higher conductivity of graphene electrode after it was coated with PEDOT:PSS, as well as the high transmittance of the thin films in the visible spectral region ($T > 90\%$, see Fig. 4b) [65].

On the other hand, Choi et al. [35] investigated a single-layer graphene-coated glass substrate acting as a transparent bottom anode. The authors discovered that the performance of the device with a structure of graphene-coated glass substrate/PEDOT:PSS/$MAPBI_3$/C_{60}/BCP/LiF/Al could not be evaluated (see Fig. 5a) because neither PESOT:PSS nor perovskite solutions could wet the hydrophobic graphene surface to form a uniform thin film (see Fig. 5b). Through interfacial engineering by incorporating 2 nm of molybdenum trioxide (MoO_3) hole transporting material (HTM) on top of the graphene electrode surface, the device performance could be improved to achieve efficiencies of up to 17.1%. The dramatic increase in the device performance was attributed to (1) the use of MoO_3 HTM, which provided hydrophilicity to the graphene surface (see Fig. 5c) and (2) the formation of desirable energy level alignment between the MoO_3/-graphene electrode and PEDOT:PSS (see Fig. 5d, e).

Later, Choi et al. [67] used the same structure on a flexible polyethylene naphthalate (PEN) substrate (PEN/-graphene/MoO_3/PEDOT:PSS/$MAPbI_3$/C_{60}/BCP/LiF/Al) and evaluated its operational stability against repeated bending. Under strain-free conditions, the device with a graphene

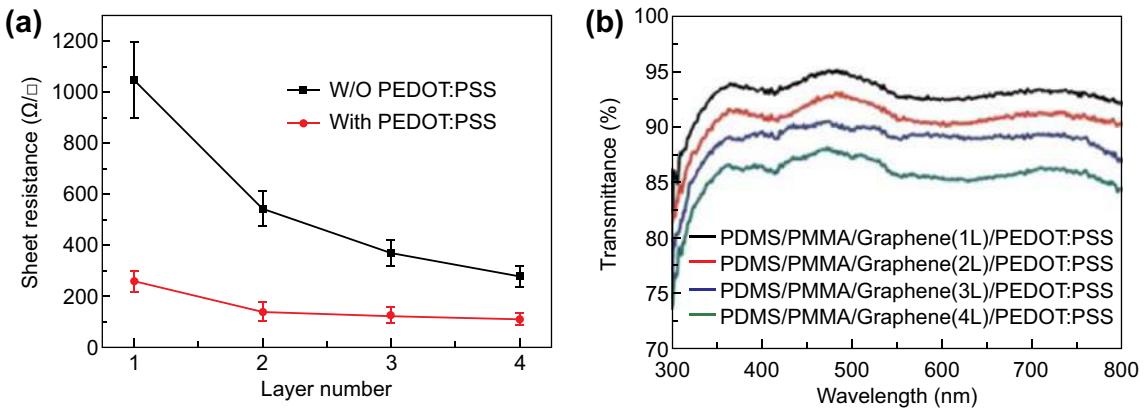

Fig. 4 **a** Sheet resistance and **b** transmittance spectra of CVD-produced graphene films (one to four layers) before and after being doped with PEDOT:PSS. Reprinted with permission from Ref. [65] Copyright 2015 John Wiley & Sons, Inc

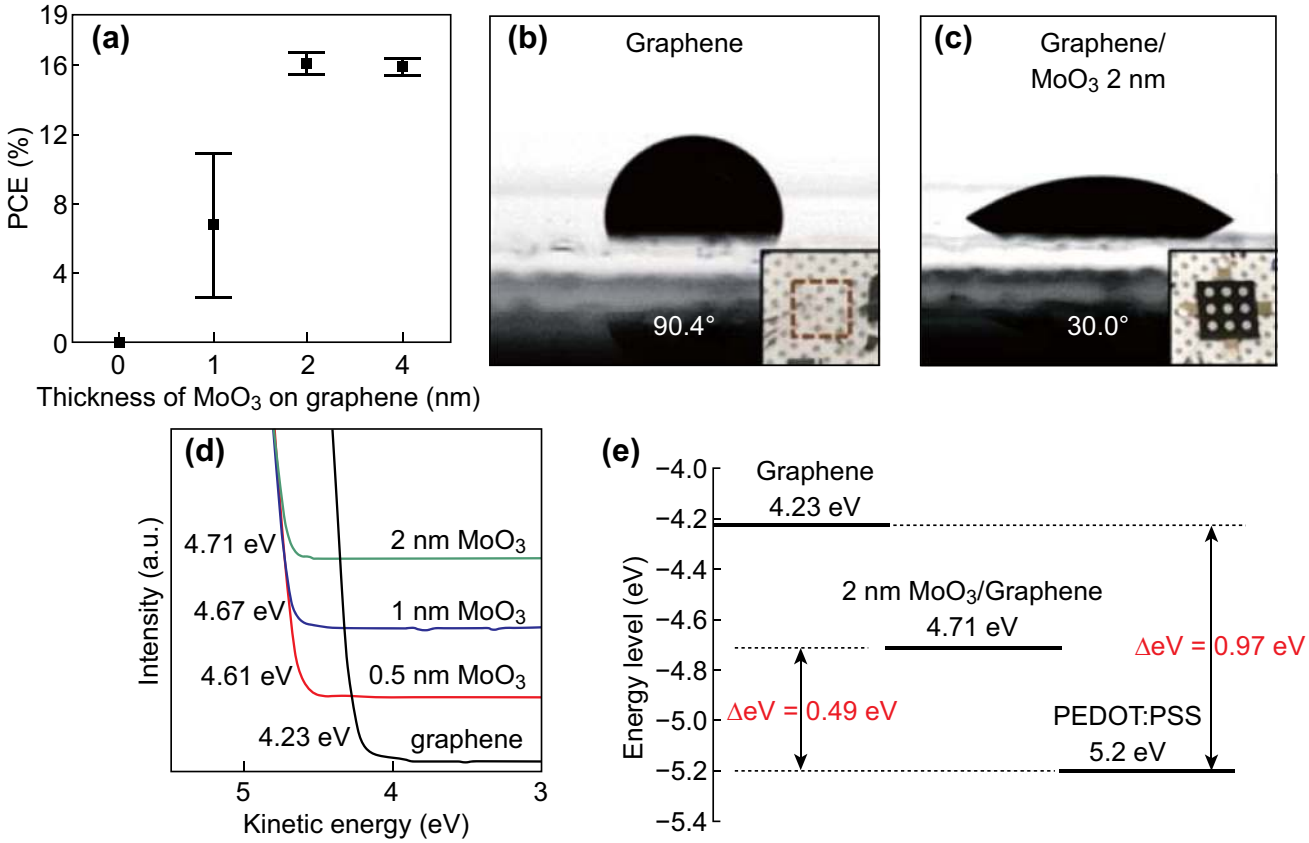

Fig. 5 **a** Average device performance with various thicknesses of MoO_3 HTM on graphene **b** Contact angle measurement using PEDOT:PSS on pristine graphene surface and **c** 2 nm of MoO_3/graphene surface. The insets in **b** and **c** are the optical images of PEDOT:PSS/$MAPbI_3$ films coated on the corresponding graphene-coated glass substrate. The MoO_3 layers were deposited in a square shape at the center of the substrates before spin-coating of PEDOT:PSS/$MAPbI_3$ thin films. **d** Work function of the graphene surface before and after being coated with MoO_3 HTM, which has been extracted from the UPS spectra. Reprinted with permission from Ref. [35] Copyright 2016 John Wiley & Sons, Inc. **e** Energy level alignment of PEDOT:PSS, graphene, and 2 nm MoO_3/graphene

conductive electrode exhibited a PCE of 16.8%, which was kept within ~ 90% of the initial value after it had been bent 1000 times at $R = 6$, 4, and 2 mm (see Fig. 6a). This can be attributed to the use of the graphene-based conductive electrode; as a result, no signs of damage were observed on the graphene or perovskite thin film surfaces under bending conditions (see Fig. 6b). In contrast, indium-doped tin oxide (ITO)-based flexible PSCs [70, 71]

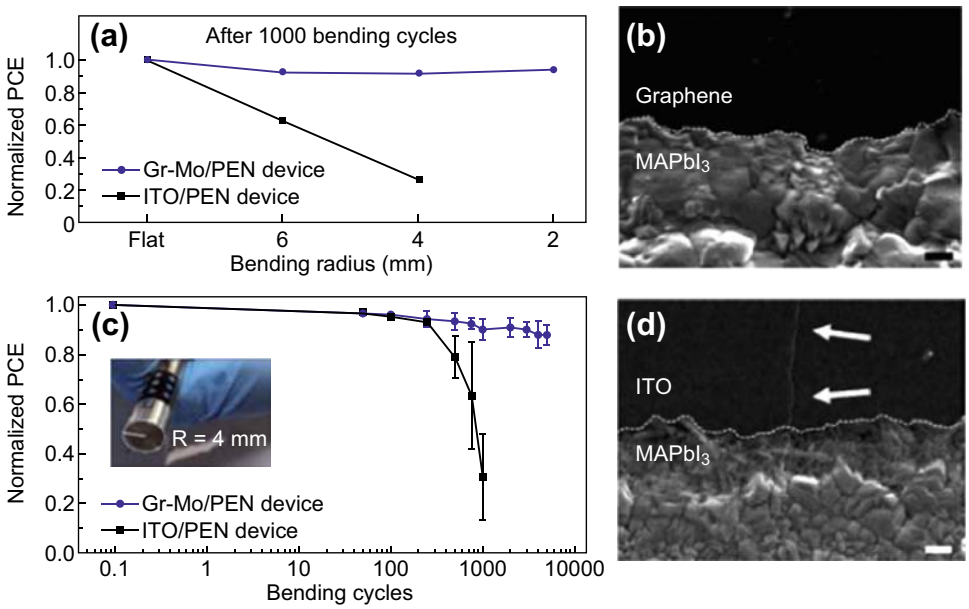

Fig. 6 Normalized PCE of graphene-MoO_3/PEN and ITO/PEN devices measured **a** after 1000 bending cycles at radii of flat, 2, 4, and 6 mm and **c** as a function of bending cycles at a fixed bending radius of 4 mm. Cross-sectional SEM images of $MAPBI_3$ perovskite films coated on **b** PEN/ITO/PEDOT:PSS and **d** PEN/Graphene-MoO_3/PEDOT:PSS after 1000 bending cycles at the bending radius of 4 mm. The scale bar is 200 nm. Reprinted with permission from Ref. [67] Copyright 2017 The Royal Society of Chemistry

showed a rapid decrease in PCE after they had been bent more than 250 times at $R = 4$ mm (see Fig. 6c); this was mainly attributed to the emergence of cracks on the brittle ITO surface, which later diffused into the perovskite thin films (see Fig. 6d). In comparison with the PEN/ITO substrate (sheet resistance $R_{sheet} = 13.3 \pm 1.3\ \Omega\ sq^{-1}$), the graphene-$MoO_3$/PEN substrate showed a higher sheet resistance of $552.0 \pm 24.2\ \Omega\ sq^{-1}$, which could reduce the charge collection efficiency of the device, leading to a high series resistance, low shunt resistance, and low the fill factor (FF). However, both devices showed similar J_{sc} values; this can be attributed to the use of the graphene-based substrate exhibiting higher transmission ($\sim$ 97% transmittance) compared to the PEN/ITO-based substrate ($\sim$ 89% transmittance) over the visible wavelength region.

On the other hand, Liu et al. [72] demonstrated a flexible PSC with a poly(3-hexylthiophene-2,5-diyl) P3HT HTM-coated graphene transparent electrode on top of a 20-µm-thick polyethylene terephthalate (PET) substrate. P3HT was used as HTM because its highest occupied molecular orbital (HOMO) level of ≈ -5.2 eV is much closer to the valence band of $MAPbI_3$ (≈ -5.4 eV) than that of conventional HTMs such as PEDOT:PSS (≈ -5.0 eV), which can facilitate hole transfer to the anode. Furthermore, it can also enhance the device stability owing to the hydrophobic nature of P3HT that does not absorb moisture in air [73, 74]. After optimizing the processing conditions by introducing $\sim$ 2-µm cross-linkable olefin-type polymer (ZEOCOAT^{TM}) as an interlayer prior to transferring the graphene layer, the device exhibited higher performance (11.5%) compared to a control device (10.4%), suggesting that the ZEOCOAT^{TM} interlayer reduced the surface roughness of the PET substrate. In addition, it was found under strain conditions that flexible devices can operate at different bending radii ($R = 0.670$, 0.365, 0.175, and 0.130 cm) with 14% degradation in device performance at the bending radius of 0.175 cm after 500 cycles [66]. Later, Heo et al. [64] demonstrated that gold chloride ($AuCl_3$)-doped graphene anode surface could extend the diffusion length of holes to the graphene electrode from $\sim$ 210 nm (control device) to $\sim$ 370 nm (champion device), where the champion device performance was enhanced by 42.1% compared to the control device.

4.2 Graphene as Carrier Transporting Material

Graphene has also been used as a carrier transporting material for PSC applications. For example, Chandrasekhar et al. [75] demonstrated that the PCE of ZnO-based PSCs could be enhanced by 47.5% from $7.01 \pm 0.66\%$ up to $10.34 \pm 0.18\%$ after graphene has been doped into the ZnO electron selective contact layer (ESCL). According to the authors, the increase in the device performance up to 48.0% can be attributed to the formation of a superior perovskite thin film (larger grains size with low surface roughness, see Fig. 7a–d) on the graphene network in the ZnO nanocrystal, which enhanced the charge carrier mobility by reducing the charge carrier recombination at

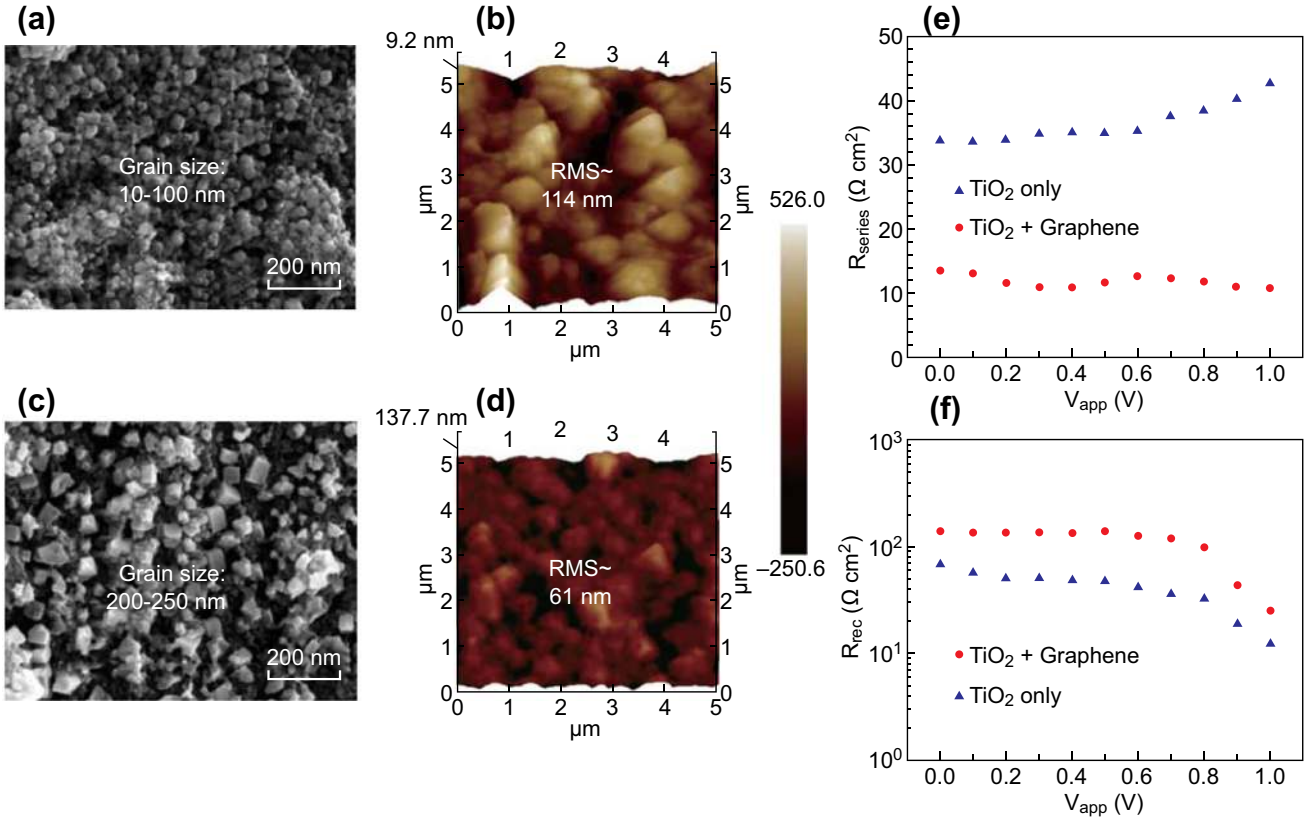

Fig. 7 SEM and AFM images of perovskite thin films prepared on ZnO films (**a**, **b**) and 0.75 wt% graphene/ZnO nanocomposite (**c**, **d**) coated glass substrates. Reprinted with permission from Ref. [75] Copyright 2017 The Royal Society of Chemistry. Series resistance **e** and recombination resistance **f** obtained from impedance spectroscopy analysis of two samples with different concentrations of graphene in TiO_2 ESCL. Reprinted with permission from Ref. [77] Copyright 2014 American Chemical Society

the defect and trap states within the perovskite layer [76]. On the other hand, Snaith et al. [77] employed graphene nanoflakes/TiO_2 nanocomposite as the ESCL and demonstrated the enhancement of the device performance (PCE = 15.6%) by 56.0% compared to the device with pure TiO_2 thin films (PCE = 10.0%).

To evaluate the role of graphene addition into TiO_2 layers, the authors performed impedance spectroscopy characterization under working cell conditions and observed that the addition of graphene into TiO_2 thin films could effectively reduce the series resistance of the device (see Fig. 7e) and charge carrier recombination rate (see Fig. 7f). In addition to binary oxides (ZnO and TiO_2), Wang et al. [78] demonstrated a graphene-doped ternary oxide-based PSC with a structure of glass/fluorine-doped tin oxide (FTO)/TiO_2/graphene-$SrTiO_3$/$MAPbI_3$/Spiro-OMeTAD/Ag. The authors showed that graphene could enhance the electron transfer rate. As a result, the optimized device exhibited a PCE of 10.49%, which was enhanced by 53.1% compared to that of a control device with a PCE of 6.85%.

To date, the highest efficiency of graphene-based PSCs has been 18.19%, which was reported by Agresti et al. [34], with an architecture of FTO-coated glass substrate/compact TiO_2/graphene-doped mesoporous TiO_2/$MAPbI_3$/graphene oxide/Spiro-OMeTad/gold. The high efficiency of the device was mainly attributed to the improved charge carrier injection/extraction and the device stability [39].

4.3 Graphene as Stabilizer Material

In addition, it is well known that perovskite thin films can be easily hydrolyzed and decomposed from dark brown into yellowish thin films under humid air environment (see Fig. 8a, b). The degradation process and decay mechanism can be described with the following equations [79]:

$$CH_3NH_3PBI_3 + H_2O \leftrightarrow CH_3NH_3PBI_3 \cdot H_2O \quad (1)$$

$$CH_3NH_3PBI_3 \cdot H_2O \leftrightarrow PBI_2 + CH_3NH_3I + H_2O \quad (2)$$

In order to solve the problem, deposition of an additional layer on top of the perovskite layer was proposed, using either a graphene layer [80] or doped with ESCL [81]

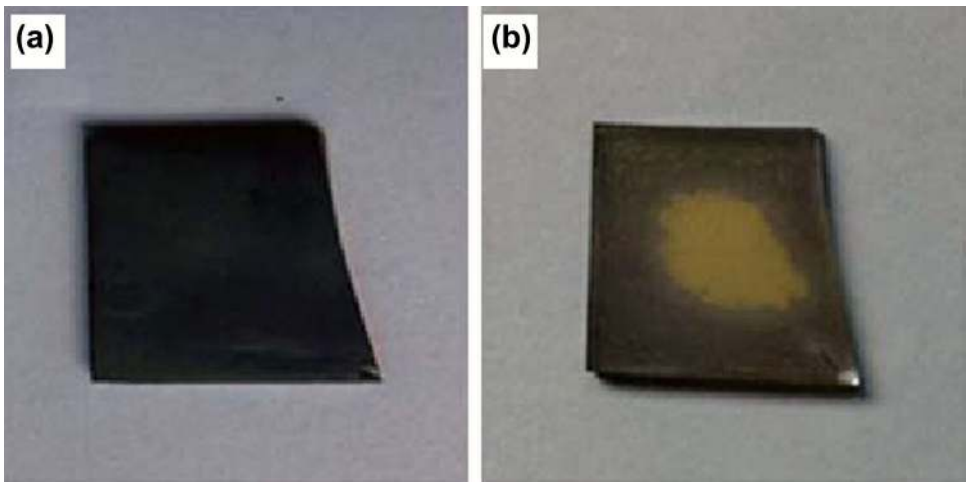

Fig. 8 Photograph images of perovskite thin films **a** before and **b** after decaying. Reprinted with permission from Ref. [79] Copyright 2016 Nature Publishing Group

/holes selective contact layer (HSCL) [82]. This is because the hydrophobic nature of graphene results in the weak affinity to moisture, and therefore, the layer can prevent the perovskite thin films from reacting with moisture in air. As a result, the diffusion of halide ions from the perovskite layer to the top electrode (Ag or Au electrode) can be inhibited [81]. The lattice parameter of 2D graphene is 0.246 nm [83], which is much smaller than the diameters of all halide anions (see Table 1). Therefore, graphene can also block the diffusion of Ag or Au atoms from the metal electrode to the perovskite thin films through the hole transporting layer [84, 85] during the thermal treatment process at ambient environment. As a result, the accordingly fabricated devices showed very good thermal and optical stabilities.

For example, Hu et al. [80] reported that CVD-produced graphene on top of perovskite/Spiro-OMeTAD thin films could retain > 94% of its original efficiency after it has been kept in 45% humidity air for 96 h or after thermal annealing at 80 °C for 12 h, even though graphene itself might reduce the hole extraction to the anode because of its lower work function of ~ 4.2 eV [35] compared to that of Spiro-OMeTAD (~ 5.2 eV) [65]. The J_{sc}, V_{oc}, FF, and PCE of the devices with (without) graphene on top of the perovskite/Spiro-OMeTAD thin films are 21.1 (21.6) mA cm^{-2}, 1.09 (1.07) V, 0.682 (0.718), and 15.7 (16.6) %, respectively. Bi et al. [81] reported that graphene-doped PCBM-based PSCs could achieve stable efficiencies of over 15% during a thermal aging test at 85 °C for 500 h or light soaking under AM 1.5 G illumination for 1000 h. Cao et al. [82] reported that graphene-doped perthiolated tri-sulfur-annulated hexa-peri-hexabenzocoronene, TSHBC, could retain 90% of its original efficiency after the device has been stored in air with a relative humidity of ~ 45% for 10 days.

5 Outlook and Conclusions

In conclusion, graphene has been used as a conductive electrode, carrier transporting material, and stabilizer material for PSC applications (Table 2). So far, CVD has been a common method to produce graphene thin films. This is because the CVD method can produce large-area graphene films and can transfer graphene onto a target substrate either by a roll-to-roll process or spin-coating method to form a conductive electrode even though it involves high-vacuum processing.

In comparison with conventional TCO-based electrodes such as FTO and indium-doped tin oxide (ITO), graphene electrodes show high flexibility and good physical, chemical, and thermal stability. Therefore, the PCE and lifetime of the devices based on graphene electrodes are much better than those of the devices based on TCO electrodes. Apart from that, graphene can enhance the electrical properties of the devices and crystallinity of the perovskite films if graphene is n-doped into metal oxide layers to act as a carrier transporting material.

To further improve the stability of PSCs, it is suggested to add a layer of graphene on top of the perovskite/hole transporting layer thin film. We believe that graphene will play an important role in PSCs in the near future. Therefore, development of novel layered graphene in different layer designs of PSCs with a controlled mechanism will be needed.

We propose to utilize oxidized or reduced graphene, in addition to pristine graphene, for PSC applications. We

Table 2 Recent development of graphene-based PSC device performance

Structure	J_{sc} (mA cm^{-2})	V_{oc} (V)	FF (%)	η (%)	Refs.
Conductive electrode					
Glass/graphene/MoO_3/PEDOT:PSS/$MAPbI_3$/C_{60}/BCP/LiF/Al	21.9[a]	1.03[a]	0.72[a]	16.1[a]	[35]
				17.1[b]	
Glass/$AuCl_3$-doped graphene/PEDOT:PSS/$MAPbI_3$/PCBM/Al	21.0[b]	1.09[b]	0.783[b]	17.9[b]	[64]
Glass/FTO/TiO_2/$MAPbI_{3-x}Cl_x$/Spiro-OMeTAD/PEDOT:PSS/graphene/PMMA/PDMS	19.17[b]	0.960[b]	0.6722[b]	12.37[b]	[65]
				12.02[a]	
PET/ZEOCOAT^{TM}/graphene/P3HT/$MAPbI_3$/PC_{71}BM/Ag	18.58[b]	1.04[b]	59.4[b]	11.48[b]	[66]
				11.27[a]	
PEN/graphene/MoO_3/PEDOT:PSS/$MAPbI_3$/C_{60}/BCP/LiF/Al	21.0[a]	0.99[a]	0.72[a]	15.0[a]	[67]
	21.7[b]	1.00[b]	0.78[b]	16.8[b]	
Carriers transporting material (CTM)					
Glass/FTO/compact TiO_2/graphene-doped mesoporous TiO_2/$MAPbI_3$/graphene oxide/Spiro-OMeTAD/Au	22.48[b]	1.08[b]	0.7512[b]	18.19[b]	[39]
				15.42[a]	
Glass/FTO/ZnO/graphene-doped ZnO/$MAPbI_3$/Spiro-OMeTAD/Ag	19.97[a]	0.926[a]	0.5631[a]	10.34[a]	[75]
Glass/FTO/graphene-doped TiO_2/Al_2O_3/$MAPBI_{3-x}Cl_x$/Spiro-OMeTAD/Au	21.9[b]	1.04[b]	0.73[b]	15.6[b]	[77]
Glass/FTO/compact TiO_2/mesoporous graphene/$SrTiO_3$/$MAPbI_3$/Spiro-OMeTAD/Ag	18.10[b]	1.00[b]	0.58[b]	10.49[b]	[78]
Stabilizer materials (SM)					
Glass/FTO/TiO_2/$MAPbI_3$/Spiro-OmeTAD/graphene/Au	21.1[b]	1.09[b]	0.682[b]	15.7[b]	[80]
Glass/FTO/NiMgLiO/$MAPbI_3$/graphene-doped PCBM/CQD/Ag	19.7[a]	1.07[a]	0.751[a]	15.8[a]	[81]
	20.6[b]	1.08[b]	0.766[b]	17.0[b]	
Glass/FTO/compact TiO_2/mesoporous TiO_2/$MAPbI_3$/graphene-coated TSHBC-R/Au	21.91[b]	0.97[b]	0.66[b]	14.02[b]	[82]

[a]Average value

[b]Best value

believe that, by optimizing the deposition process in terms of time, temperature, solvent, precursor selection, etc., new designs of PSCs with good performance and stability can be developed. Once graphene-based materials have proved to be useful in photovoltaic technologies, low-cost PSCs can be realized and commercialized in the market. Further, other optoelectronic devices will be designed follow this trend, initiating the era of low-cost optoelectronic devices.

Acknowledgements This work was financially supported by the Ministry of Higher Education (FRGS/1/2017/STG02/UKM/02/1) and Universiti Kebangsaan Malaysia (GUP-2015-019).

References

1. M.-G. Kang, M.-S. Kim, J. Kim, L.J. Guo, Organic solar cells using nanoimprinted transparent metal electrodes. Adv. Mater. **20**(23), 4408–4413 (2008). https://doi.org/10.1002/adma.200800750
2. E.L. Lim, C.C. Yap, M.A.M. Teridi, C.H. Teh, A.R.B.M. Yusoff, M.H.H. Jumali, A review of recent plasmonic nanoparticles incorporated P3HT: PCBM organic thin film solar cells. Org. Electron. **36**, 12–18 (2016). https://doi.org/10.1016/j.orgel.2016.05.029
3. S. Albrecht, B. Rech, Perovskite solar cells: on top of commercial photovoltaics. Nat. Energy **2**(1), 16196 (2017). https://doi.org/10.1038/nenergy.2016.196
4. T. Saga, Advances in crystalline silicon solar cell technology for industrial mass production. NPG Asia Mater. **2**(3), 96–102 (2010). https://doi.org/10.1038/asiamat.2010.82
5. W.A. Badawy, A review on solar cells from Si-single crystals to porous materials and quantum dots. J. Adv. Res. **6**(2), 123–132 (2015). https://doi.org/10.1016/j.jare.2013.10.001
6. A. Shah, P. Torres, R. Tscharner, N. Wyrsch, H. Keppner, Photovoltaic technology: the case for thin-film solar cells. Science **285**(5428), 692–698 (1999)
7. J.-P. Correa-Baena, A. Abate, M. Saliba, W. Tress, T. Jesper Jacobsson, M. Grätzel, A. Hagfeldt, The rapid evolution of highly efficient perovskite solar cells. Energy Environ. Sci. **10**(3), 710–727 (2017). https://doi.org/10.1039/C6EE03397K
8. A. Kojima, K. Teshima, Y. Shirai, T. Miyasaka, Organometal halide perovskites as visible-light sensitizers for photovoltaic cells. J. Am. Chem. Soc. **131**(17), 6050–6051 (2009). https://doi.org/10.1021/ja809598r

9. J.-H. Im, C.-R. Lee, J.-W. Lee, S.-W. Park, N.-G. Park, 65% efficient perovskite quantum-dot-sensitized solar cell. Nanoscale **3**(10), 4088–4093 (2011). https://doi.org/10.1039/c1nr10867k
10. M.M. Lee, J. Teuscher, T. Miyasaka, T.N. Murakami, H.J. Snaith, Supporting material: efficient hybrid solar cells based on meso-superstructured organometal halide perovskites. Science **338**, 643–647 (2012). https://doi.org/10.1126/science.1228604
11. D. Liu, T.L. Kelly, Perovskite solar cells with a planar heterojunction structure prepared using room-temperature solution processing techniques. Nat. Photon. **8**(2), 133–138 (2013). https://doi.org/10.1038/nphoton.2013.342
12. W.S. Yang, J.H. Noh, N.J. Jeon, Y.C. Kim, S. Ryu, J. Seo, S.I. Seok, Solar cells, high-performance photovoltaic perovskite layers fabricated through intramolecular exchange. Science **348**(6240), 1234–1237 (2015). https://doi.org/10.1126/science.aaa9272
13. M. Saliba, T. Matsui, J.-Y. Seo, K. Domanski, J.-P. Correa-Baena et al., Cesium-containing triple cation perovskite solar cells: improved stability, reproducibility and high efficiency. Energy Environ. Sci. **9**(6), 1989–1997 (2016). https://doi.org/10.1039/C5EE03874J
14. W.S. Yang, B.-W. Park, E.H. Jung, N.J. Jeon, Y.C. Kim et al., Iodide management in formamidinium-lead-halide-based perovskite layers for efficient solar cells. Science **356**(6345), 1376–1379 (2017). https://doi.org/10.1126/science.aan2301
15. K. Hwang, Y.S. Jung, Y.J. Heo, F.H. Scholes, S.E. Watkins, J. Subbiah, D.J. Jones, D.Y. Kim, D. Vak, Toward large scale roll-to-roll production of fully printed perovskite solar cells. Adv. Mater. **27**(7), 1241–1247 (2015). https://doi.org/10.1002/adma.201404598
16. R. Søndergaard, M. Hösel, D. Angmo, T.T. Larsen-Olsen, F.C. Krebs, Roll-to-roll fabrication of polymer solar cells. Mater. Today **15**(1–2), 36–49 (2012). https://doi.org/10.1016/S1369-7021(12)70019-6
17. M.A. Green, Y. Hishikawa, W. Warta, E.D. Dunlop, D.H. Levi, J. Hohl-Ebinger, A.W.H. Ho-Baillie, Solar cell efficiency tables (version 50). Prog. Photovolt. Res. Appl. **25**, 668–676 (2017). https://doi.org/10.1002/pip.2909
18. N. Cheng, P. Liu, F. Qi, Y. Xiao, W. Yu, Z. Yu, W. Liu, S.S. Guo, X.Z. Zhao, Multi-walled carbon nanotubes act as charge transport channel to boost the efficiency of hole transport material free perovskite solar cells. J. Power Sources **332**, 24–29 (2016). https://doi.org/10.1016/j.jpowsour.2016.09.104
19. J.-I. Park, J.H. Heo, S.-H. Park, K. Il Hong, H.G. Jeong, S.H. Im, H.-K. Kim, Highly flexible InSnO electrodes on thin colourless polyimide substrate for high-performance flexible $CH_3NH_3PbI_3$ perovskite solar cells. J. Power Sources **341**, 340–347 (2017). https://doi.org/10.1016/j.jpowsour.2016.12.026
20. W. Zhang, J. Xiong, S. Wang, W. Liu, J. Li, D. Wang, H. Gu, X. Wang, J. Li, Highly conductive and transparent silver grid/metal oxide hybrid electrodes for low-temperature planar perovskite solar cells. J. Power Sources **337**, 118–124 (2017). https://doi.org/10.1016/j.jpowsour.2016.10.101
21. C. Zhang, Y. Luo, X. Chen, Y. Chen, Z. Sun, S. Huang, Effective improvement of the photovoltaic performance of carbon-based perovskite solar cells by additional solvents. Nano-Micro Lett. **8**, 347–357 (2016). https://doi.org/10.1007/s40820-016-0094-4
22. F. Giordano, A. Abate, J.P. Correa Baena, M. Saliba, T. Matsu et al., Enhanced electronic properties in mesoporous TiO_2 via lithium doping for high-efficiency perovskite solar cells. Nat. Commun. **7**, 10379 (2016). https://doi.org/10.1038/ncomms10379
23. X. Zhao, H. Shen, Y. Zhang, X. Li, X. Zhao et al., Aluminum-doped zinc oxide as highly stable electron collection layer for perovskite solar cells. ACS Appl. Mater. Interfaces. **8**(12), 7826–7833 (2016). https://doi.org/10.1021/acsami.6b00520
24. Y. Bai, Y. Fang, Y. Deng, Q. Wang, J. Zhao, X. Zheng, Y. Zhang, J. Huang, Low temperature solution-processed Sb: SnO_2 nanocrystals for efficient planar perovskite solar cells. Chemsuschem **9**(18), 2686–2691 (2016). https://doi.org/10.1002/cssc.201600944
25. B.-X. Chen, H.-S. Rao, W.-G. Li, Y.-F. Xu, H.-Y. Chen, D.-B. Kuang, C.-Y. Su, Achieving high-performance planar perovskite solar cell with Nb-doped TiO_2 compact layer by enhanced electron injection and efficient charge extraction. J. Mater. Chem. A **4**(15), 5647–5653 (2016). https://doi.org/10.1039/C6TA00989A
26. X. Li, M.I. Dar, C. Yi, J. Luo, M. Tschumi, S.M. Zakeeruddin, M.K. Nazeeruddin, H. Han, M. Grätzel, Improved performance and stability of perovskite solar cells by crystal crosslinking with alkylphosphonic acid ω-ammonium chlorides. Nat. Chem. **7**(9), 703–711 (2015). https://doi.org/10.1038/nchem.2324
27. C. Liu, W. Ding, X. Zhou, J. Gao, C. Cheng, X.-Z. Zhao, B. Xu, Efficient and stable perovskite solar cells prepared in ambient air based on surface-modified perovskite layer. J. Phys. Chem. C **121**(12), 6546–6553 (2017). https://doi.org/10.1021/acs.jpcc.7b00847
28. Y. Zhang, J. Wang, J. Xu, W. Chen, D. Zhu, W. Zheng, X. Bao, Efficient inverted planar formamidinium lead iodide perovskite solar cells via post improve perovskite layer. RSC Adv. **6**(83), 79952 (2016). https://doi.org/10.1039/C6RA15210D
29. S.S. Mali, C.S. Shim, H. Kim, P.S. Patil, C.K. Hong, *In situ* processed gold nanoparticle-embedded TiO_2 nanofibers enabling plasmonic perovskite solar cells to exceed 14% conversion efficiency. Nanoscale **8**(5), 2664–2677 (2016). https://doi.org/10.1039/C5NR07395B
30. A.E. Shalan, T. Oshikiri, H. Sawayanagi, K. Nakamura, K. Ueno, Q. Sun, H.-P. Wu, E.W.-G. Diau, H. Misawa, Versatile plasmonic-effects at the interface of inverted perovskite solar cells. Nanoscale **9**(3), 1229–1236 (2017). https://doi.org/10.1039/C6NR06741G
31. M. Long, Z. Chen, T. Zhang, Y. Xiao, X. Zeng, J. Chen, K. Yan, J. Xu, Ultrathin efficient perovskite solar cells employing a periodic structure of a composite hole conductor for elevated plasmonic light harvesting and hole collection. Nanoscale **8**(12), 6290–6299 (2016). https://doi.org/10.1039/C5NR05042A
32. K. Chan, M. Wright, N. Elumalai, A. Uddin, S. Pillai, Plasmonics in organic and perovskite solar cells: optical and electrical effects. Adv. Opt. Mater. **5**(6), 1600698 (2017). https://doi.org/10.1002/adom.201600698
33. J.-S. Yeo, R. Kang, S. Lee, Y.-J. Jeon, N. Myoung et al., Highly efficient and stable planar perovskite solar cells with reduced graphene oxide nanosheets as electrode interlayer. Nano Energy **12**(12), 96–104 (2015). https://doi.org/10.1016/j.nanoen.2014.12.022
34. A. Agresti, S. Pescetelli, L. Cinà, D. Konios, G. Kakavelakis, E. Kymakis, A. Di Carlo, Efficiency and stability enhancement in perovskite solar cells by inserting lithium-neutralized graphene oxide as electron transporting layer. Adv. Funct. Mater. **26**(16), 2686–2694 (2016). https://doi.org/10.1002/adfm.201504949
35. H. Sung, N. Ahn, M.S. Jang, J.-K. Lee, H. Yoon, N.-G. Park, M. Choi, Transparent conductive oxide-free graphene-based perovskite solar cells with over 17% efficiency. Adv. Energy Mater. **6**(3), 1501873 (2016). https://doi.org/10.1002/aenm.201501873
36. Q.-D. Yang, J. Li, Y. Cheng, H.-W. Li, Z. Guan, B. Yu, S.-W. Tsang, Graphene oxide as an efficient hole-transporting material for high-performance perovskite solar cells with enhanced stability. J. Mater. Chem. A **5**, 9852–9858 (2017). https://doi.org/10.1039/C7TA01752A
37. H. Luo, X. Lin, X. Hou, L. Pan, S. Huang, X. Chen, Efficient and air-stable planar perovskite solar cells formed on graphene-oxide-modified PEDOT:PSS hole transport layer. Nano-Micro Lett. **9**, 39 (2017). https://doi.org/10.1007/s40820-017-0140-x

38. M. Batmunkh, C.J. Shearer, M.J. Biggs, J.G. Shapter, Nanocarbons for mesoscopic perovskite solar cells. J. Mater. Chem. A **3**(17), 9020–9031 (2015). https://doi.org/10.1039/C5TA00873E
39. A. Agresti, S. Pescetelli, B. Taheri, A.E. Del Rio Castillo, L. Cinà, F. Bonaccorso, A. Di Carlo, Graphene–perovskite solar cells exceed 18% efficiency: a stability study. Chemsuschem **9**(18), 2609–2619 (2016). https://doi.org/10.1002/cssc.201600942
40. K.S. Novoselov, A.K. Geim, S.V. Morozov, D. Jiang, Y. Zhang, S.V. Dubonos, I.V. Grigorieva, A.A. Firsov, Electric field effect in atomically thin carbon films. Science **306**, 666–669 (2004). https://doi.org/10.1126/science.1102896
41. X. Wan, Y. Huang, Y. Chen, Focusing on energy and optoelectronic applications: a journey for graphene and graphene oxide at large scale. Acc. Chem. Res. **45**(4), 598–607 (2012). https://doi.org/10.1021/ar200229q
42. A.A. Balandin, S. Ghosh, W. Bao, I. Calizo, D. Teweldebrhan, F. Miao, C.N. Lau, Superior thermal conductivity of single-layer graphene. Nano Lett. **8**(3), 902–907 (2008). https://doi.org/10.1021/nl0731872
43. K.I. Bolotin, K.J. Sikes, Z. Jiang, M. Klima, G. Fudenberg, J. Hone, P. Kim, H.L. Stormer, Ultrahigh electron mobility in suspended graphene. Solid State Commun. **146**(9–10), 351–355 (2008). https://doi.org/10.1016/j.ssc.2008.02.024
44. R.R. Nair, P. Blake, A.N. Grigorenko, K.S. Novoselov, T.J. Booth, T. Stauber, N.M.R. Peres, A.K. Geim, Fine structure constant defines visual transparency of graphene. Science **320**(5881), 1308 (2008). https://doi.org/10.1126/science.1156965
45. M.D. Stoller, S. Park, Y. Zhu, J. An, R.S. Ruoff, Graphene-based ultracapacitors. Nano Lett. **8**(10), 3498–3502 (2008). https://doi.org/10.1021/nl802558y
46. C. Lee, X. Wei, J.W. Kysar, J. Hone, Measurement of the elastic properties and intrinsic strength of monolayer graphene. Science **321**(5887), 385–388 (2008). https://doi.org/10.1126/science.1157996
47. Y. Shao, J. Wang, H. Wu, J. Liu, I.A. Aksay, Y. Lin, Graphene based electrochemical sensors and biosensors: a review. Electroanalysis **22**(10), 1027–1036 (2010). https://doi.org/10.1002/elan.200900571
48. N.M. Julkapli, S. Bagheri, Graphene supported heterogeneous catalysts: an overview. Int. J. Hydrog. Energy **40**(2), 948–979 (2015). https://doi.org/10.1016/j.ijhydene.2014.10.129
49. M. Liu, X. Yin, X. Zhang, Double-layer graphene optical modulator. Nano Lett. **12**(3), 1482–1485 (2012). https://doi.org/10.1021/nl204202k
50. W. Xu, N. Mao, J. Zhang, Graphene: a platform for surface-enhanced Raman spectroscopy. Small **9**(8), 1206–1224 (2013). https://doi.org/10.1002/smll.201203097
51. F. Bonaccorso, Z. Sun, T. Hasan, A.C. Ferrari, Graphene photonics and optoelectronics. Nat. Photon. **4**(9), 611–622 (2010). https://doi.org/10.1038/nphoton.2010.186
52. H. Kim, J.H. Ahn, Graphene for flexible and wearable device applications. Carbon **120**, 244–257 (2017). https://doi.org/10.1016/j.carbon.2017.05.041
53. J. Zhang, X. Yang, H. Deng, K. Qiao, U. Farooq et al., Low-dimensional halide perovskites and their advanced optoelectronic applications. Nano-Micro Lett. **9**, 36 (2017). https://doi.org/10.1007/s40820-017-0137-5
54. J. Liang, C. Wang, Y. Wang, Z. Xu, Z. Lu et al., All-inorganic perovskite solar cells. J. Am. Chem. Soc. **138**(49), 15829–15832 (2016). https://doi.org/10.1021/jacs.6b10227
55. I. Borriello, G. Cantele, D. Ninno, *Ab initio* investigation of hybrid organic–inorganic perovskites based on tin halides. Phys. Rev. B **77**(23), 235214 (2008). https://doi.org/10.1103/PhysRevB.77.235214
56. Z. Li, M. Yang, J.-S. Park, S.-H. Wei, J. Berry, K. Zhu, Stabilizing perovskite structures by tuning tolerance factor: formation of formamidinium and cesium lead iodide solid-state alloys. Chem. Mater. **28**(1), 284–292 (2016). https://doi.org/10.1021/acs.chemmater.5b04107
57. C.H. Yoder, *Ionic Compounds: Applications of Chemistry to Mineralogy*. In Ionic Compounds. (Wiley, New York, 2006), p. 171. https://doi.org/10.1002/0470075104.app3
58. Z. Fan, K. Sun, J. Wang, Perovskites for photovoltaics: a combined review of organic–inorganic halide perovskites and ferroelectric oxide perovskites. J. Mater. Chem. A **3**(37), 18809–18828 (2015). https://doi.org/10.1039/C5TA04235F
59. C. Zheng, O. Rubel, Ionization energy as a stability criterion for halide perovskites. J. Phys. Chem. C **121**(22), 11977–11984 (2017). https://doi.org/10.1021/acs.jpcc.7b00333
60. M. Pandey, K.W. Jacobsen, K.S. Thygesen, Band gap tuning and defect tolerance of atomically thin two-dimensional organic–inorganic halide perovskites. J. Phys. Chem. Lett. **7**(21), 4346–4352 (2016). https://doi.org/10.1021/acs.jpclett.6b01998
61. A. Miyata, A. Mitioglu, P. Plochocka, O. Portugall, J.T.-W. Wang, S.D. Stranks, H.J. Snaith, R.J. Nicholas, Direct measurement of the exciton binding energy and effective masses for charge carriers in organic–inorganic tri-halide perovskites. Nat. Phys. **11**(7), 582–587 (2015). https://doi.org/10.1038/nphys3357
62. K. Galkowski, A. Mitioglu, A. Miyata, P. Plochocka, O. Portugall et al., Determination of the exciton binding energy and effective masses for methylammonium and formamidinium lead tri-halide perovskite semiconductors. Energy Environ. Sci. **9**(3), 962–970 (2016). https://doi.org/10.1039/C5EE03435C
63. V. Gonzalez-Pedro, E.J. Juarez-Perez, W.-S. Arsyad, E.M. Barea, F. Fabregat-Santiago, I. Mora-Sero, J. Bisquert, General working principles of $CH_3NH_3PbX_3$ perovskite solar cells. Nano Lett. **14**(2), 888–893 (2014). https://doi.org/10.1021/nl404252e
64. J.H. Heo, D.H. Shin, S. Kim, M.H. Jang, M.H. Lee, S.W. Seo, S.-H. Choi, S.H. Im, Highly efficient $CH_3NH_3PbI_3$ perovskite solar cells prepared by $AuCl_3$-doped graphene transparent conducting electrodes. Chem. Eng. J. **323**, 153–159 (2017). https://doi.org/10.1016/j.cej.2017.04.097
65. P. You, Z. Liu, Q. Tai, S. Liu, F. Yan, Efficient semitransparent perovskite solar cells with graphene electrodes. Adv. Mater. **27**(24), 3632–3638 (2015). https://doi.org/10.1002/adma.201501145
66. Z. Liu, P. You, C. Xie, G. Tang, F. Yan, Ultrathin and flexible perovskite solar cells with graphene transparent electrodes. Nano Energy **28**, 151–157 (2016). https://doi.org/10.1016/j.nanoen.2016.08.038
67. J. Yoon, H. Sung, G. Lee, W. Cho, N. Ahn, H.S. Jung, M. Choi, Superflexible, high-efficiency perovskite solar cells utilizing graphene electrodes: towards future foldable power sources. Energy Environ. Sci. **10**(1), 337–345 (2017). https://doi.org/10.1039/C6EE02650H
68. F. Guo, H. Azimi, Y. Hou, T. Przybilla, M. Hu et al., High-performance semitransparent perovskite solar cells with solution-processed silver nanowires as top electrodes. Nanoscale **7**(5), 1642–1649 (2015). https://doi.org/10.1039/C4NR06033D
69. Z. Li, S.A. Kulkarni, P.P. Boix, E. Shi, A. Cao et al., Laminated carbon nanotube networks for metal electrode-free efficient perovskite solar cells. ACS Nano **8**(7), 6797–6804 (2014). https://doi.org/10.1021/nn501096h
70. B.J. Kim, D.H. Kim, Y.-Y. Lee, H.-W. Shin, G.S. Han et al., Highly efficient and bending durable perovskite solar cells: toward a wearable power source. Energy Environ. Sci. **8**(3), 916–921 (2015). https://doi.org/10.1039/C4EE02441A
71. J.H. Heo, M.H. Lee, H.J. Han, B.R. Patil, J.S. Yu, S.H. Im, Highly efficient low temperature solution processable planar type $CH_3NH_3PbI_3$ perovskite flexible solar cells. J. Mater. Chem. A **4**(5), 1572–1578 (2016). https://doi.org/10.1039/C5TA09520D

72. H. Kim, K.-G. Lim, T.-W. Lee, Planar heterojunction organometal halide perovskite solar cells: roles of interfacial layers. Energy Environ. Sci. **9**(1), 12–30 (2016). https://doi.org/10.1039/C5EE02194D
73. G.-W. Kim, G. Kang, M.M. Byranvand, G.-Y. Lee, T. Park, Gradated mixed hole transport layer in a perovskite solar cell: improving moisture stability and efficiency. ACS Appl. Mater. Interfaces. **9**(33), 27720–27726 (2017). https://doi.org/10.1021/acsami.7b07071
74. J. Xiao, J. Shi, H. Liu, Y. Xu, S. Lv, Y. Luo, D. Li, Q. Meng, Y. Li, Efficient $CH_3NH_3PbI_3$ perovskite solar cells based on graphdiyne (GD)-modified P3HT hole-transporting material. Adv. Energy Mater. **5**(8), 1401943 (2015). https://doi.org/10.1002/aenm.201401943
75. P.S. Chandrasekhar, V.K. Komarala, Graphene/ZnO nanocomposite as an electron transport layer for perovskite solar cells; the effect of graphene concentration on photovoltaic performance. RSC Adv. **7**, 28610–28615 (2017). https://doi.org/10.1039/C7RA02036H
76. C.-M. Liu, C.-M. Chen, Y.-W. Su, S.-M. Wang, K.-H. Wei, The dual localized surface plasmonic effects of gold nanodots and gold nanoparticles enhance the performance of bulk heterojunction polymer solar cells. Org. Electron. **14**(10), 2476–2483 (2013). https://doi.org/10.1016/j.orgel.2013.06.012
77. J.T.-W. Wang, J.M. Ball, E.M. Barea, A. Abate, J.-A. Webber et al., Low-temperature processed electron collection layers of graphene/TiO_2 nanocomposites in thin film perovskite solar cells. Nano Lett. **14**(2), 724–730 (2014). https://doi.org/10.1021/nl403997a
78. C. Wang, Y. Tang, Y. Hu, L. Huang, J. Fu, J. Jin, W. Shi, L. Wang, W. Yang, Graphene/$SrTiO_3$ nanocomposites used as an effective electron-transporting layer for high-performance perovskite solar cells. RSC Adv. **5**(64), 52041–52047 (2015). https://doi.org/10.1039/C5RA09001F
79. J. Zhao, B. Cai, Z. Luo, Y. Dong, Y. Zhang et al., Investigation of the hydrolysis of perovskite organometallic halide $CH_3NH_3PbI_3$ in humidity environment. Sci. Rep. **6**, 21976 (2016). https://doi.org/10.1038/srep21976
80. X. Hu, H. Jiang, J. Li, J. Ma, D. Yang, Z. Liu, F. Gao, S.F. Liu, Air and thermally stable perovskite solar cells with CVD-graphene as the blocking layer. Nanoscale **9**(24), 8274–8280 (2017). https://doi.org/10.1039/C7NR01186E
81. E. Bi, H. Chen, F. Xie, Y. Wu, W. Chen et al., Diffusion engineering of ions and charge carriers for stable efficient perovskite solar cells. Nat. Commun. **8**, 15330 (2017). https://doi.org/10.1038/ncomms15330
82. J. Cao, Y.-M. Liu, X. Jing, J. Yin, J. Li, B. Xu, Y.-Z. Tan, N. Zheng, Well-defined thiolated nanographene as hole-transporting material for efficient and stable perovskite solar cells. J. Am. Chem. Soc. **137**(34), 10914–10917 (2015). https://doi.org/10.1021/jacs.5b06493
83. T. Ohta, A. Bostwick, T. Seyller, K. Horn, E. Rotenberg, Controlling the electronic structure of bilayer graphene. Science **313**(5789), 951–954 (2006). https://doi.org/10.1126/science.1130681
84. A. Guerrero, J. You, C. Aranda, Y.S. Kang, G. Garcia-Belmonte, H. Zhou, J. Bisquert, Y. Yang, Interfacial degradation of planar lead halide perovskite solar cells. ACS Nano **10**(1), 218–224 (2016). https://doi.org/10.1021/acsnano.5b03687
85. K. Domanski, J.P. Correa-Baena, N. Mine, M.K. Nazeeruddin, A. Abate, M. Saliba, W. Tress, A. Hagfeldt, M. Grätzel, Not all that glitters is gold: metal-migration-induced degradation in perovskite solar cells. ACS Nano **10**(6), 6306–6314 (2016). https://doi.org/10.1021/acsnano.6b02613